Supplementary Information

Role of Microstructure in the Electron-Hole Interaction of Hybrid Lead-Halide Perovskites

Giulia Grancini[1‡], Ajay Ram Srimath Kandada[1‡], Jarvist M. Frost[2], Alex J. Barker[1], Michele De Bastiani[1,3], Marina Gandini[1], Sergio Marras[4], Guglielmo Lanzani[1], Aron Walsh[2] and Annamaria Petrozza[1]*

* annamaria.petrozza@iit.it

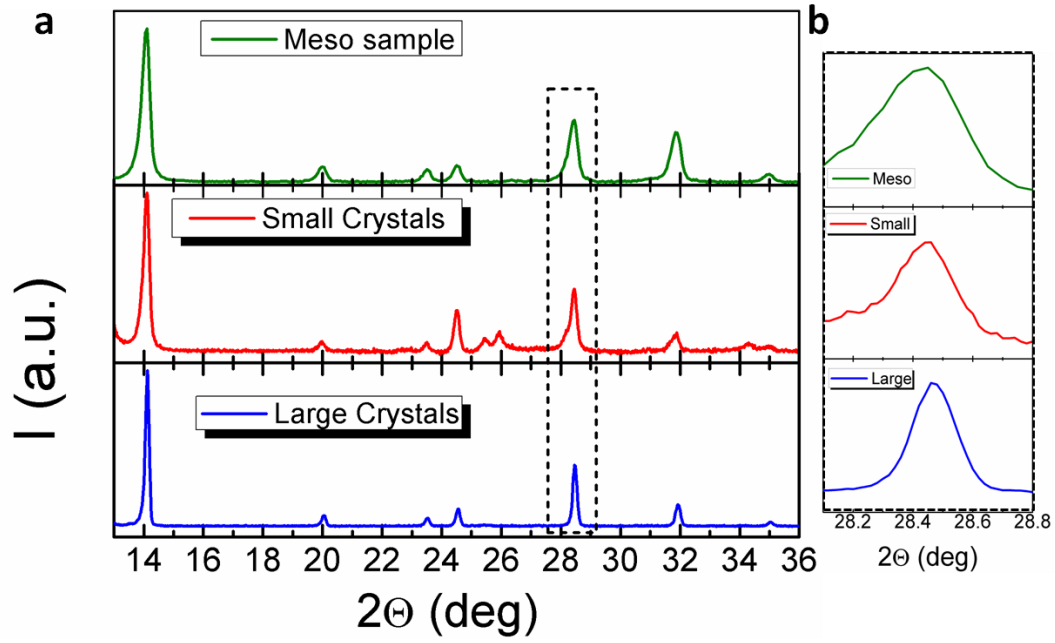

Figure S1| a. XRD patterns of $MAPbI_3$ thin films (top panel) grown in 3μm alumina meso-scaffold, thus comprising a meso phase and a capping layer and

corresponding to the sample investigated in Figure 1 of the manuscript, (middle panel) sample made of “small crystals” (corresponding to the sample shown in Figure 2a) and (bottom panel) sample made of “large crystals” (corresponding to the sample shown in Figure 2b).**b.** zoom of Figure S2a of the peak at 28.4.

X-ray diffraction measurements from the perovskite provide evidence for any changes to the crystal size. The XRD patterns shown in Figure S1 belong to the “meso” sample, consisting of a $MAPbI_3$ infiltrated in a thick mesoporous alumina substrate with capping layer (Figure 1 of the main manuscript) and to the thin films with “small” and “large” crystals reported in Figure 2 a, b, respectively. The peak positions are in agreement with the previous report of the $MAPbI_3$ perovskite in tetragonal phase [1]. The average size of the crystalline domains can be estimated from the full-width at half maximum (FWHM) of those peaks using the Scherrer equation (as reported in the legend of the Table S1). The instrumental broadening effect was removed using a diffraction pattern collected from a NIST LaB_6 (SRM 660) standard. XRD Data analysis was carried out using PDXL 2.1 software from Rigaku. From a simple visual inspection one can immediately notice a reduction the broadening of the peaks (see inset in Figure S1b) going from the “meso” sample to the “large crystals” sample. This clearly indicates that the average size of the crystalline domains increases. This qualitative trend is in agreement with the increase in the crystals dimension observed from the SEM images, reflecting the properties of the average dimension of the crystalline domains they are constituted by.

Table S1 Results of average crystallite size calculated using Scherrer equation $D_{hkl} = K\lambda / (B_{hkl} \cos\theta)$, where D_{hkl} is crystallite size in the direction perpendicular to the lattice planes; hkl: miller indices of the planes being analyzed; K = crystallite shape factor = 0.94; λ = wavelength of the X-rays; B_{hkl} = FWHM (in radians) and θ = Bragg angle. Note that the value for the meso sample is an average of two distributions of crystalline domains, the ones confined in the mesoporous scaffold, along with the ones aggregated forming the capping layer, thus the number reported is surely overestimated.

	Meso Sample	**Sample A**	**Sample B**
Fitted Size (nm)	32 (+-2)	45(+-4)	135(+-7)

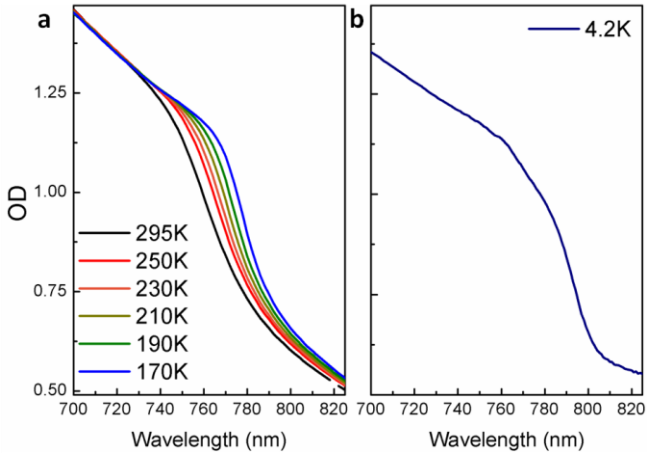

Figure S2| Temperature dependent UV-VIS Absorption of the meso 3μm thick $MAPbI_3$ sample in **a.** the [295 K - 170 K] range and **b.** at 4.2 K.

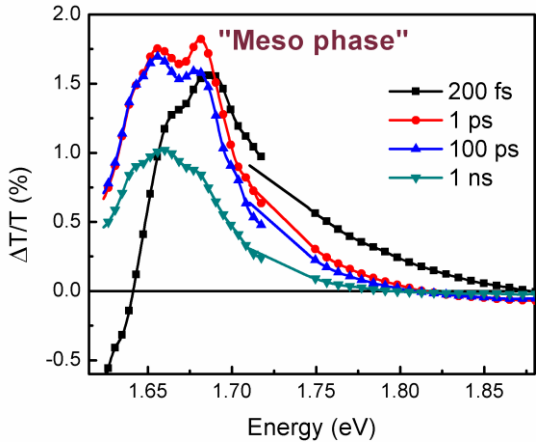

Figure S3| TA spectral evolution between 200 fs and 1 ns at 295 K of “meso phase”. The optical absorption spectrum is shown in solid line.

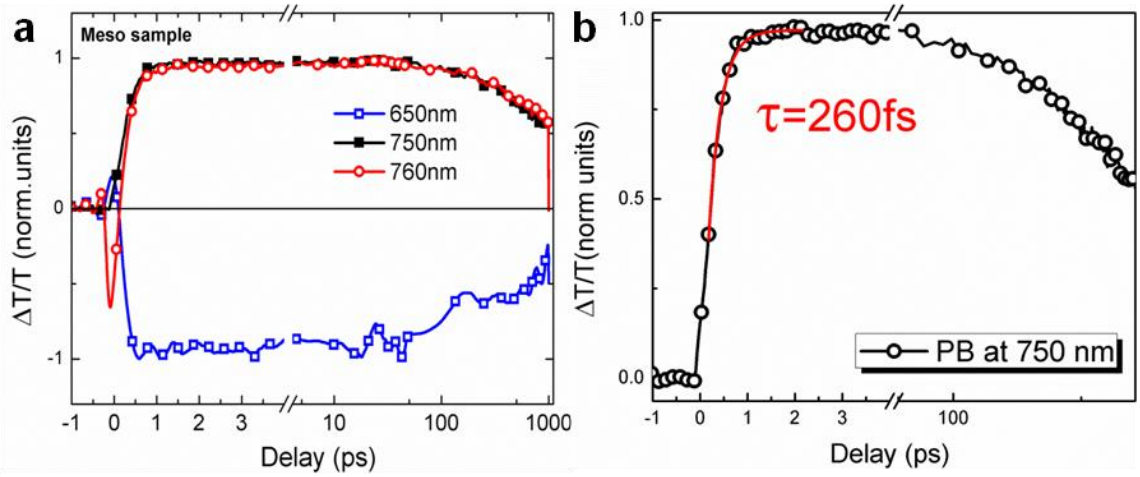

Figure S4| a, TA dynamics of the meso $MAPbI_3$ sample at probed wavelength indicated in the legend. **b,** Exponential fit of the rising PB signal at 750 nm, giving a time constant of 260 fs.

Figure S3 shows the TA spectral evolution between 200 fs and 1 ns obtained after photoexcitation at 520 nm (2.38 eV, well above the conduction band edge). At 200 fs pump-probe delay, we observe : 1) a broad positive band ($\Delta T/T > 0$) peaking at ~ 1.67 eV close to the optical band edge, that we assign to a photo-bleach (PB) band due to the state filling. Dynamics (shown in Figure S4) show the rise of the PB with a time constant of 260 fs following the hot-carrier thermalization to the bottom of the conduction band; 2) a sharp photo-induced absorption (PA_2) band peaking at ~1.61 eV. It is at the red edge of the PB. PA_2 arises from the spectral modulation of the optical absorption due to the Coulomb interaction between the photoexcited carriers. This effect is generally described as carrier-induced Stark effect or band gap renormalization in inorganic semiconductors. On longer times, as the hot-carriers thermalize, PB at 1.67 eV grows in intensity, overwhelming this effect; 3) a weak and broad negative band in blue region, PA_1 above 1.85 eV that we tentatively assign to a change in the dielectric constant, agreement with [2]. Essentially, all these TA spectral features suggest a free carrier picture in this sample, without any excitonic contributions.

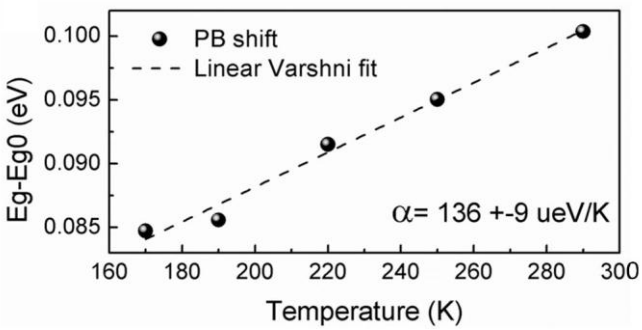

Figure S5| Energy gap shift with temperature fitted by the linear Varshni's law. For most semiconductors (e.g. GaAs) the gap shifts to lower energies with increasing temperature. Pb-based compounds have an exceptional behavior. In PbS films, for example, lattice dilation contributes increasing the band gap. Similar to PbS, $MAPI_3$ also has a band gap determined at the boundary of the first Brillouin zone, which results in this non-conventional behavior. The energy gap (E_g) dependence on temperature follows the empirical law $E_g=E_0-\alpha T^2/(T+\beta)$ (1) where E_0 represents the material energy gap at T=0, while α and β are constant parameters characteristic of a given material. In the high temperature regime taken into account, equation (1) can be approximated by a linear function of T: $E_g(T)=E_g(0)-dE_g/dT*T$. A linear fit to the changes in the PB spectral position (Fig 1c in the main text) allows us to estimate $dE_g/dT=136$ μeV/K.

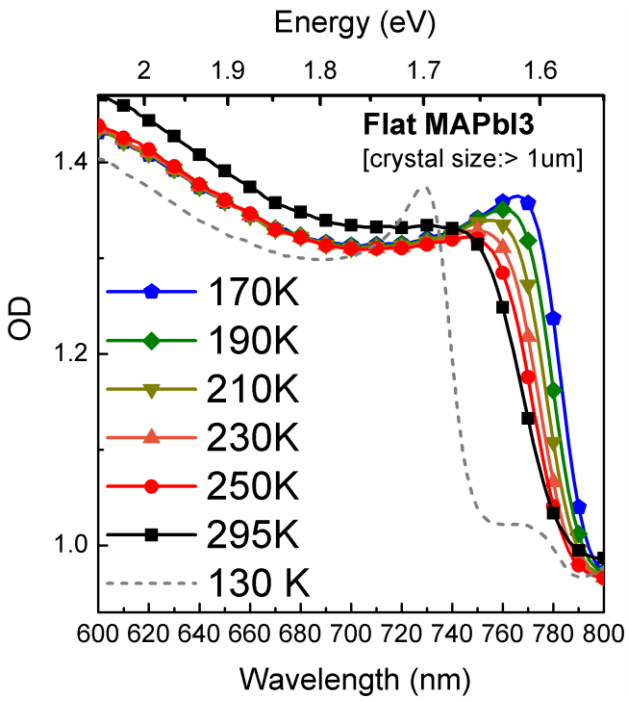

Figure S6| absorption spectra from 295K and to 130K -after phase transition- of the perovskite film with crystallites of ~ 1μm average size (see SEM image in Fig 2b of the manuscript).

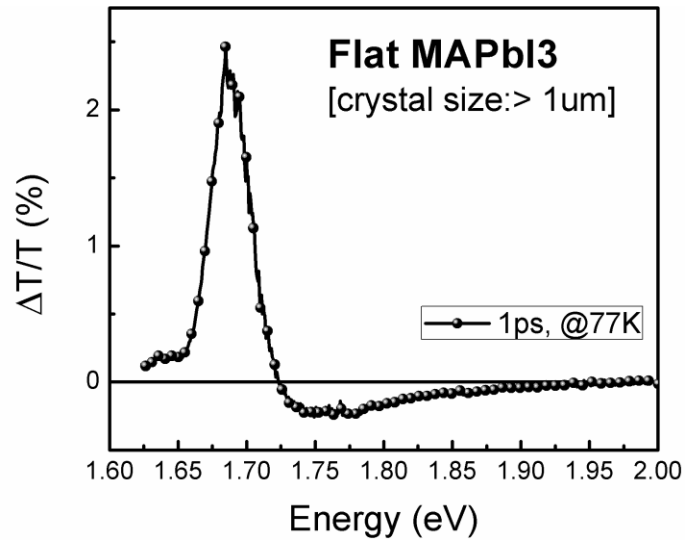

Figure S7| TA spectra at 77K (below the tetragonal-to-orthorhombic phase) at 1 ps pump-probe delay of the perovskite film with crystal size above 1μm on average. The spectrum clearly shows the derivative shape and the negative MA* band, in fully agreement with the excitonic picture observed for purely excitonic system [4,5].

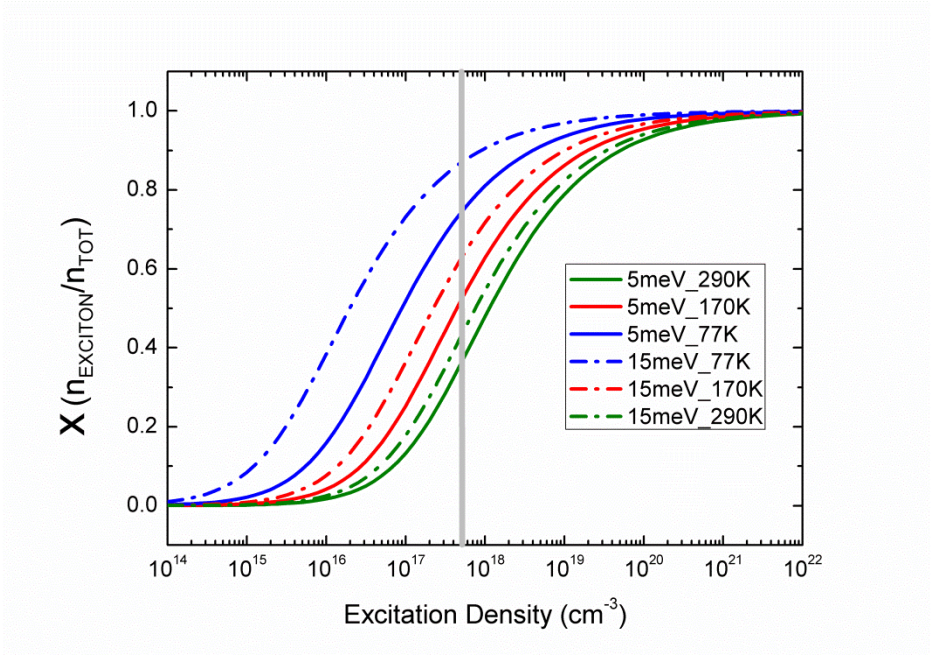

Figure S8| Simulation of Exciton fraction at thermal equilibrium using Saha Equation. The plot shows the fraction of excitons as a function of excitation density at various temperatures (RT, 170 K and 77 K) and at two values of exciton binding energy (5meV and 15 meV) which have been taken from Miyata, A. *et al.* in. *Nat. Phys.* 11, 582-587 (2015). For details of the simulations, see [3]. The grey line indicates the photo-excitation density used in the TA experiments reported in the manuscript. It is evident from the above plot that even with the lowest binding energy of 5 meV and at 170 K, exciton fraction can be as large as 50%, considerable enough to give perceivable TA signatures. However, since the simulation involves several assumptions/approximations, it should be considered only as guideline and not as a quantitative support in the TA analysis.

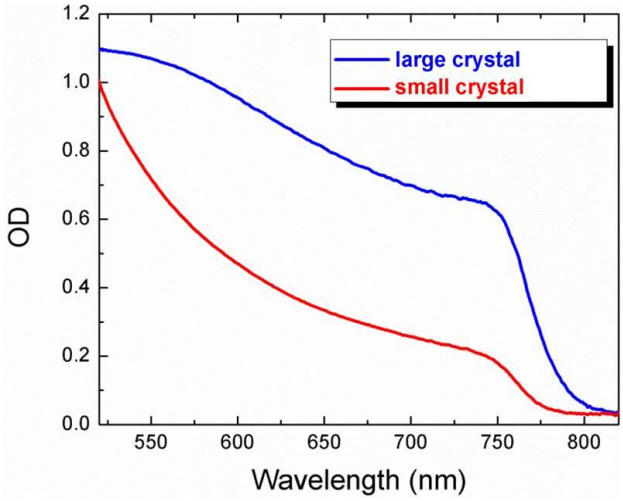

Figure S9| Absorption spectra at 295K of the flat perovskite film with crystallites of < 200 nm (red line) and ~ 1µm (blue line) average size (same samples presented in Fig.2 a, b, respectively).

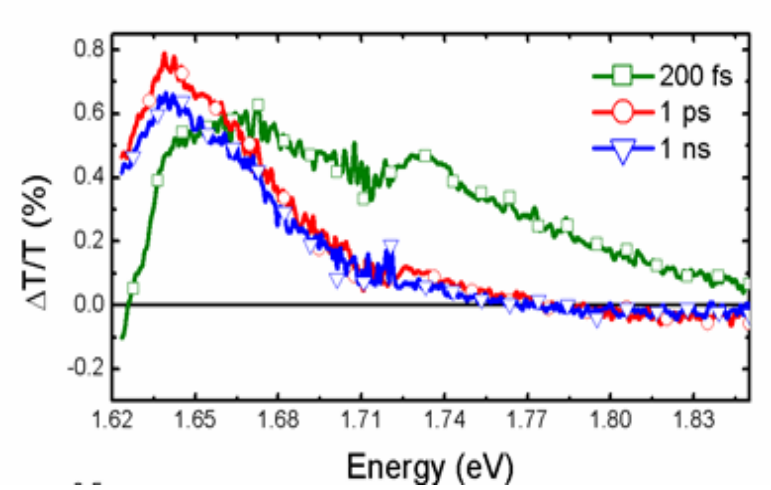

Figure S10| TA spectral evolution between 200fs and 1ns at 295K of the sample shown in Fig 2a in the main manuscript.

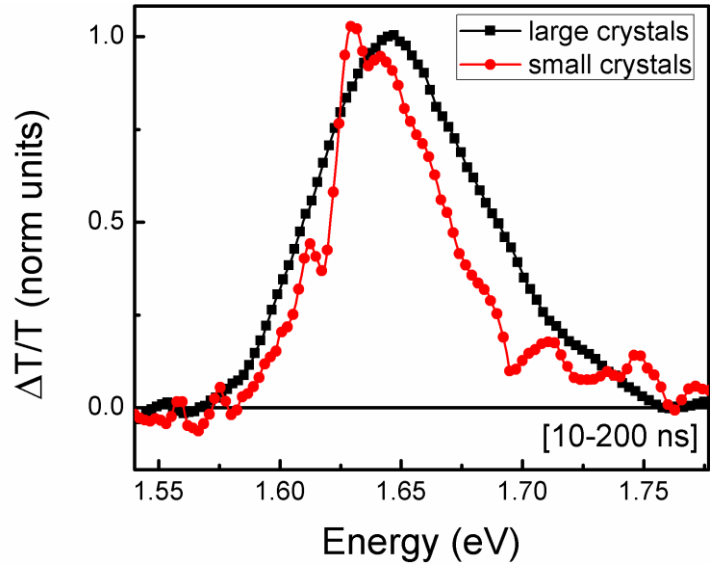

Figure S11| TA spectra at 295K integrated in [10-200 ns] range of the flat perovskite film with crystal size of < 200 nm (red dots) and ~ 1μm (black squares) (same samples presented in Fig.2 a, b, respectively).

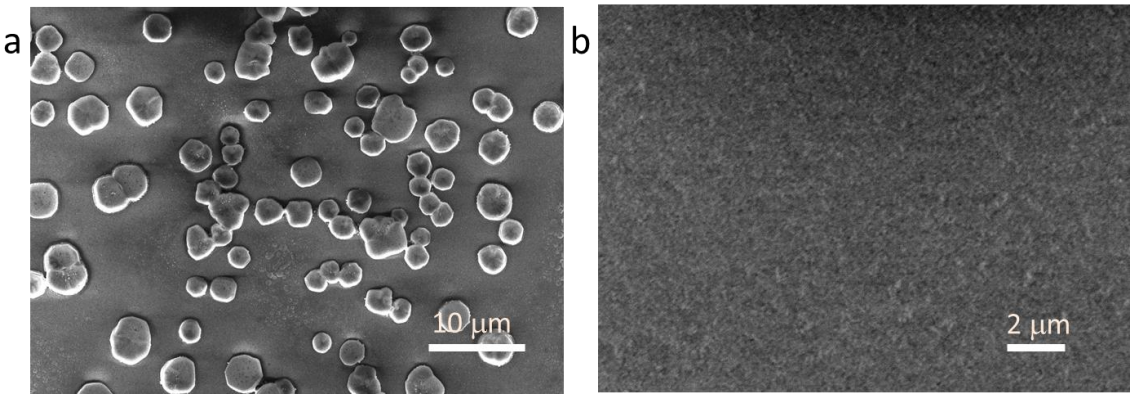

Figure S12| SEM images of MAPbBr3 perovskite films. The perovskite is deposited on (a) glass substrate forming average crystallite dimension ~1μm; (b) Al_2O_3 scaffold.

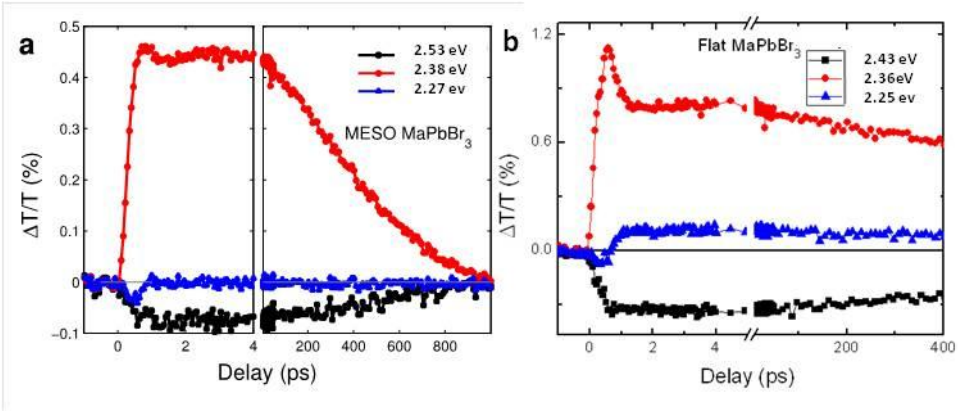

Figure S13| TA dynamics of the a) small and b) large $MAPbBr_3$ crystallites sample at probed wavelengths as indicated in the legend(the relative spectra are shown in Figure 3 of the main manuscript).

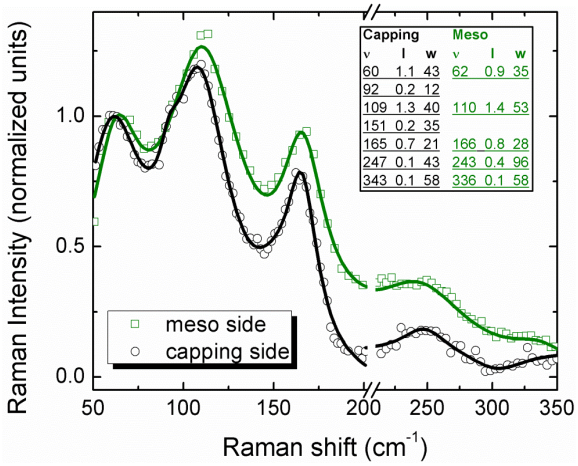

Figure S14| Resonant Raman spectra of "meso-3μm" $MAPbI_3$ upon excitation from the meso phase (green line) and from the capping side (black line); the thick solid lines represent the results of the fit from a multi-peaks Gaussian functions. The broadening and a red-shift of the torsional vibration of the cations at around 250 cm^{-1} is the signature of cation ordering in the inorganic cage, while the reduction of the relative intensity of the 120 cm^{-1} /90 cm^{-1} peaks is the

signature of a reduction in the Pb-I bond strain. Excitation at 532 nm. Table with fitting parameters as inset.

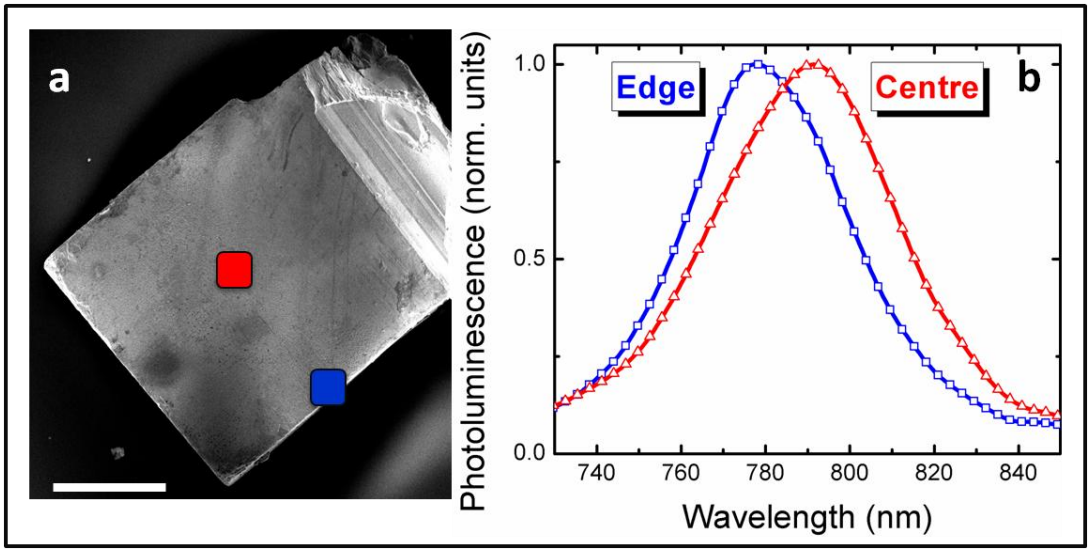

Figure S15 a. SEM image of the single crystal (0.5mm*0.5mm), scalebar: 200μm; **b.** microscopic PL spectra obtained moving from the edge (blue line) to the center (red line) of the crystal face in the spot indicated in Figure S15a. A 20x objective has been used to focus the excitation beam down to a micrometer-large spot. There is a clear red shift of around 30meV of the optical edge moving from the edge to the centre suggesting energetic dishomogeneity within the single crystal. Details on sample fabrication can be found in *E. Hoke et al. Chem. Sci., 2015, 6, 613*.

Experimental methods:

X-ray diffraction (XRD).

XRD patterns were recorded with a Rigaku SmartLab X-Ray diffractometer equipped with a 9 kW CuKα rotating anode, operating at 40 kV and 150 mA. A Göbel mirror was used to convert the divergent X-ray beam into a parallel beam and to suppress the Cu Kβ radiation (1.392 Å). The diffraction patterns were collected at room temperature in a symmetric scan reflection mode.

Raman set-up:

The micro Raman system is based on an optical microscope (Renishaw microscope, equipped with 5×, 20×, 50× and 100× short and long working distance microscope objectives) used to focus the excitation light and collect it in a back scattering configuration, a monochromator, notch filters system and a charge coupled detector. The sample is mounted on a translation stage of a Leica microscope. The excitation used consists of a diode laser at 532 nm. The system has been calibrated against the 520.5 cm-1 line of an internal silicon wafer. The spectra have been registered in the 60-300 cm-1 range, particularly sensitive to the Pb-I modes. The final data have been averaged over hundred accumulations in order to maximize the signal to noise ratio. The measurements were conducted at room temperature and in air. The laser power intensity has been kept of the order of 300 μW in order to avoid any sample degradation effects.

Nanosecond Transient Absorption

Nanosecond transient absorption measurements were carried out with a LP920 laser flash spectrometer (Edinburgh Instruments). It is based on a standard "pump-probe" setup where the sample is excited by a ns laser pulse (pump) and the time evolution of the differential absorption changes induced by the pump is monitored by a second weak probe generated by a cw light source. The pump pulses are provided by a nanosecond tunable OPOLett-355II laser (10 Hz repetition rate). The probe light is provided by a pulsed Xenon arc lamp. The sample was kept at a 45° angle to the excitation beam. The beams are focused onto the sample ensuring the spatial overlap. The transmitted probe is spectrally filtered by a monochromator and detected. Two different detection systems are used: a cooled ICCD camera which enables to detect the entire spectral range from 350 to 850 nm at once and a set of photomultipliers (with both VIS and near-IR detection window) enabling one to collect the single-wavelength kinetic with higher sensitivity. The signal is finally recorded by recorded by a TDS 3032C digital signal analyzer. From the transmission change following photoexcitation the variation in the absorption is thus derived as:

$$\Delta OD(\tau,\lambda) = \frac{\log(I_{probe})}{I_t(\tau,\lambda)} \qquad (\mathbf{1})$$

where I_{probe} is the transmitted probe with excitation off and I_t is the transmitted probe after laser excitation. The system has sensitivity of $5 \cdot 10^{-4}$ and a temporal resolution of 7 ns.

References

[1]N. J. Jeon, J. H. Noh, Y. C. Kim, W. S. Yang, S. Ryu, S. I. Seok, Nat. Materials 13, 897 (2014).

[2] F. Deschler, M.Price,.S. Pathak,.L. E. Klintberg,.D. D.Jarausch,R. Higler, S. Huttner, T. Leijtens, S. D. Stranks, H. J. Snaith, M. Atature, R.T. Phillips, R.H. Friend, *J. Phys. Chem. Lett.* **5**, 1421−1426 (2014).

[3] D'Innocenzo, V. *et al.* Excitons versus free charges in organo-lead tri-halide perovskites. *Nat. Commun.* **5,** 3486 (2014).

[3] Peyghambarian, N. *et al.* Blue shift of the exciton resonance due to exciton-exciton interactions in a multiple-quantum-well structure. *Phys. Rev. Lett.* **53,** 2433–2436 (1984).

[4] Shimizu, M., Fujisawa, J.-I. & Ishi-Hayase, J. Influence of dielectric confinement on excitonic nonlinearity in inorganic-organic layered semiconductors. *Phys. Rev. B* **71,** 205306 (2005).